

NASA Technical Memorandum 106038  
 ICOMP-93-2

IN-34  
 151054  
 P.29

# Structure of Confined Laminar Spray Diffusion Flames/Numerical Investigation

M.A. Mawid  
*Institute for Computational Mechanics in Propulsion*  
*Lewis Research Center*  
*Cleveland, Ohio*

D.L. Bulzan  
*Lewis Research Center*  
*Cleveland, Ohio*

and

S.K. Aggarwal  
*The University of Illinois at Chicago*  
*Chicago, Illinois*

*and Institute for Computational Mechanics in Propulsion*  
*Lewis Research Center*  
*Cleveland, Ohio*

February 1993

**NASA**

N93-22596

Unclass

G3/34 0151054

(NASA-TM-106038) STRUCTURE OF  
 CONFINED LAMINAR SPRAY DIFFUSION  
 FLAMES: NUMERICAL INVESTIGATION  
 (NASA) 29 p





## Structure of Confined Laminar Spray Diffusion Flames/Numerical Investigation

M.A. Mawid  
Institute for Computational Mechanics in Propulsion  
NASA Lewis Research Center  
Cleveland, Ohio

D.L. Bulzan  
NASA Lewis Research Center  
Cleveland, Ohio

and

S.K. Aggarwal  
The University of Illinois at Chicago  
Chicago, Illinois  
and Institute for Computational Mechanics in Propulsion  
NASA Lewis Research Center  
Cleveland, Ohio

### ABSTRACT

The structure of confined laminar spray diffusion flames is investigated numerically by solving the gas-phase conservation equations for mass species, continuity, momentum, and energy and the liquid-phase equations for droplet position, velocity, size, and temperature. A one-step global reaction scheme along with six equilibrium reactions are employed to model the flame chemistry. Monodisperse as well as polydisperse sprays are considered. The numerical results demonstrate that liquid spray flames substantially differ from gaseous flames in their structure, i.e., temperature, concentration, and velocity fields, shape, and dimensions under the same conditions. Spray flames are predicted to be taller and narrower than their counterpart gaseous ones and their shapes are almost cylindrical, in agreement with experimental observations. The numerical computations also show that the use of the equilibrium reactions with the one-step reaction scheme decreases the flame temperature compared to the one-step reaction scheme without the equilibrium reactions and more importantly increases the surface area of the flame zone due to a phenomenon termed "equilibrium broadening". The spray flames also possess a finite thickness with minimal overlap of the fuel and oxygen species. A case, for which a fuel-mixture consisting of 20-80% gas-liquid by mass is introduced into the combustor, is also investigated and compared with predictions using only gaseous or liquid fuel.

## I. INTRODUCTION

Much of the current understanding of the physical and chemical processes occurring in combusting flows has resulted from studies of diffusion flames. This began with the development of laminar gaseous diffusion flame theory by Burke and Shumann<sup>1</sup>. The apparatus used to produce the gaseous flame consisted of two concentric tubes. An inner tube in which the combustible gas flows in and an outer tube through which air flows. With this theory of diffusion flames, Burke and Shumann were able to predict certain important flame characteristics such as flame shape and height using some restrictive assumptions such as a constant and uniform velocity field, and mixing is only due to radial diffusion. Attempts to refine the Burke-Shumann model have been made by a number of investigators<sup>2-7</sup>. In all cases, however, the refinements aimed towards relaxing some of the restrictive assumptions made by Burke and Shumann in order to obtain a better physical description of the diffusion flame.

The stumbling block that prevented a more realistic and complete representation of diffusion flames has been the strong coupling between the fluid dynamics and chemistry. This precluded the attainment of an analytic solution to this class of diffusion flames. Therefore, a detailed solution, which accounts for most of these physical and chemical processes and their interactions, can *only* be sought numerically.

Several numerical investigations<sup>8-11</sup> have been conducted to simulate laminar confined and unconfined gaseous diffusion flames. These investigations differed from each other in the method for modeling certain aspects of the physical and chemical processes. The concept of a flame sheet, for example, was adopted to represent the flame front<sup>8-9</sup>. A global one-reaction finite chemistry model was also used<sup>10-11</sup>. A fairly complete representation of temperature, concentration, and velocity fields in laminar gaseous diffusion flames emerged from these numerical investigations. In particular, it was shown<sup>10</sup> that gaseous diffusion

flames do possess a finite thickness and due to gas expansion, some important radial flow is induced which in turn enhances mixing. Large scale instabilities in the oxidizer region of the flame were predicted<sup>11</sup> when gravity was included in the computations.

All the aforementioned studies have considered *only* a gaseous fuel jet issuing either from an orifice into a free environment or through a cylindrical tube similar to the Burke-Shumann setting. In many realistic situations, however, diffusion flames are formed by injecting a liquid fuel spray from an atomizer<sup>12-14</sup>. Burning of a liquid fuel in a spray flame is quite different from that of a pure gaseous fuel. Because, in general, the presence of liquid fuel droplets of various sizes and velocities affects the entire velocity field and consequently flame characteristics. Understanding the stabilization mechanism of spray flames relies considerably on understanding the velocity field structure of the region near the flame front. In addition, drop sizes, velocities, and relative velocities in spray flames determine vaporization rate, drag forces, and drop trajectories and thus concentration, velocity, and temperature fields. These important issues were not addressed in the original theory of Burke and Shumann and in the analyses that followed.

Experimental and theoretical efforts have been made in order to understand the effects of introducing the fuel in the form of liquid and/or partially liquid on the flame structure and stabilization mechanism. Moore and Moore<sup>15</sup> investigated theoretically and experimentally a confined laminar diffusion flame supported by a low-momentum iso-octane spray. In their theoretical model, they retained all the assumptions made by Burke and Shumann for the gas-phase and the liquid drops were assumed to move with local gas velocity. Limited agreement between the theoretical and experimental results was obtained. In a similar study, Harsha and Edelman<sup>16</sup> developed an analytic model for an unconfined spray diffusion flame. Overall satisfactory agreement with experimental results of Mao et al.<sup>17</sup> was established. Kim and Sichel<sup>18</sup> obtained an analytical solution for a Burke-Shumann type experiment in which a liquid fuel jet and an oxidizer gas moved in

parallel at the same speed. Their results also show some limited qualitative agreement with experimental observations.

Recently Greenberg<sup>19</sup> reexamined analytically the classical Burke-Shumann flat diffusion flame, assuming that the fuel is introduced partly in the form of liquid droplets suspended homogeneously in an inert gas stream and the remainder as a gas. The fundamental assumptions of Burke-Shumann's theory were retained with the exception of allowing for axial diffusion and the presence of liquid droplets. One striking result obtained, when the liquid droplets as well as the gaseous fuel were allowed to flow in the inner tube, is that the flame was about 30% shorter and 15% narrower than its counterpart gaseous diffusion flame under the same conditions. The model, however, failed to predict the flame shape and other characteristics when *only* liquid fuel was present in the inner tube. In a latter study, Greenberg<sup>20</sup> removed a fundamental assumption, made earlier<sup>19</sup>, concerning the fluid dynamics of the spray droplets. That is that spray droplets were permitted to have different velocities from that of the gas; thus allowing relative velocity between droplets and the surrounding gas. Other assumptions such as flame sheet and instantaneous droplet-gas temperature adjustment were, however, retained. Flames almost twice as tall as that of Burke-Shumann were predicted when 80% of the fuel was supplied as a liquid. Results, allowing only for liquid fuels, once again were not reported.

An investigation of the fundamental processes involved in laminar spray flames cannot be realized analytically. Apart from the few analytical treatises of the classical Burke-Shumann diffusion flame with liquid fuel spray, the literature contains *no numerical contribution* on the subject of laminar spray diffusion flames. All the previous analytical studies were partial and did not provide a complete representation of the concentration, temperature, and velocity fields. Moreover, no information on droplet behavior in the spray flame was provided. It is the objective of this study to perform a comprehensive numerical investigation of a laminar spray diffusion flame. This would shed light not only

upon the structure and characteristics of liquid flames as opposed to that of gaseous ones but also upon the mechanism of their own stability. Although the effect of gravity is not considered in the present investigation, the results of this study will assist experimentalists to observe that under the conditions of the present study, stabilized laminar spray flames can be established. This is important, since there have been concerns reported<sup>21</sup>, regarding the experimental difficulty associated with stabilizing liquid spray flames in laminar flows.

In the present study, the gas-phase equations for overall mass continuity, species mass continuity, momentum, and energy, and the liquid-phase equations for droplet position, velocity, size, and temperature are solved numerically. The exchange processes of mass, momentum, and energy between the two phases are accounted for as source/sink terms in the gas-phase governing equations. The computations are two-dimensional axisymmetric and the numerical modeling is performed using the KIVA-II<sup>22</sup> computational algorithm. The governing equations are given in the next section followed by sections on numerical procedure, results and discussions, and conclusion respectively.

## II. GOVERNING EQUATIONS

Figure 1 shows a schematic of the physical model considered in the present study. It consists of two concentric tubes, with nitrogen in the inner tube of radius  $L=0.5$  cm and air in the outer tube of radius  $R=2$  cm. The liquid droplets are injected through the inner tube along the axis of symmetry. The radial distance is represented by  $r$  and the vertical distance, measured from the end of the tube AA, is denoted by  $Z$ . The governing equations are written in vector form and the differential operators are referenced with respect to a Cartesian coordinate system. They are given below:

### Gas-Phase Equations:

### Mass Species Continuity

$$\frac{\partial \rho_i}{\partial t} + \vec{\nabla} \cdot (\rho_i \vec{u}) = \vec{\nabla} \cdot (\rho D \vec{\nabla} Y_i) + \rho_{ic} + \rho_{is} \quad (1)$$

Where  $\rho_i$  is the partial mass density of the  $i$ th species,  $\rho$  total fluid density,  $Y_i$  mass fraction of the  $i$ th species,  $t$  time,  $\vec{u}$  fluid velocity, and  $\rho_{ic}$  and  $\rho_{is}$  are chemistry and spray source terms defined in Appendix A. Note that all source/sink terms due to spray and chemical reactions are defined in Appendix A.  $D$  is the diffusion coefficient, assumed to be the same for all species exclusive of the fuel species, and is related to the fluid viscosity,  $\mu$ , through the Schmidt number,  $Sc$ , as

$$D = \frac{\mu}{\rho Sc}$$

### Overall Mass Continuity

$$\frac{\partial \rho}{\partial t} + \vec{\nabla} \cdot (\rho \vec{u}) = \rho_s \quad (2)$$

### Momentum

$$\frac{\partial \rho \vec{u}}{\partial t} + \vec{\nabla} \cdot (\rho \vec{u} \vec{u}) = -\vec{\nabla} P + \vec{\nabla} \cdot \vec{\sigma} + \vec{F}_s \quad (3)$$

where  $P$  is the fluid pressure and  $\vec{\sigma}$  is the viscous stress tensor expressed as

$$\vec{\sigma} = \mu [\vec{\nabla} \vec{u} + (\vec{\nabla} \vec{u})^T] + \lambda \vec{\nabla} \cdot \vec{u}$$

$\mu$  and  $\lambda$  are the first and second viscosity coefficients and the superscript T denotes the transpose. A Sutherland formula is used for the molecular viscosity of air

$$\mu_a = \frac{A_1 T^{3/2}}{T + A_2}$$

$T$  is the fluid temperature and  $A_1$  and  $A_2$  are constants.  $\vec{F}_s$  is the momentum exchange term due to spray defined in Appendix A.

### Energy

$$\frac{\partial \rho I}{\partial t} + \vec{\nabla} \cdot (\rho \vec{u} I) = -P \vec{\nabla} \cdot \vec{u} - \vec{\nabla} \cdot \vec{J} + Q_c + Q_s \quad (4)$$



$I$  is the specific internal energy and  $\vec{J}$  is the heat flux given by

$$\vec{J} = -K\vec{\nabla}T - \sum_i h_i(\rho D\vec{\nabla}Y_i)$$

The thermal conductivity  $K$  is related to Prandtl number,  $Pr$ , through

$$K = \frac{\mu C_p}{Pr}$$

where  $C_p$  and  $h_i$  are respectively the fluid specific heat and enthalpy of the  $i$ th species. Note that Schmidt and Prandtl numbers are assumed to be constant and are unity and 0.7 respectively.  $Q_c$  and  $Q_s$  are source terms due to chemical reactions and spray. The equation of state and the state relations are

$$P = R_u \rho T \sum_i Y_i / W_i \quad (5)$$

$R_u$  is the universal gas constant and  $W_i$  is the molecular weight of the  $i$ th species. Total energy, specific heat and the  $i$ th species enthalpy are

$$I(T) = \sum_i Y_i I_i(T) \quad (6)$$

$$C_p(T) = \sum_i Y_i C_{p_i}(T) \quad (7)$$

$$h_i(T) = I_i(T) + R_u T / W_i \quad (8)$$

The values of  $h_i(T)$  and  $C_{p_i}$  are obtained from the JANAF table<sup>23</sup>.

### Liquid-Phase Equations:

As a liquid droplet travels in the gas stream, it exchanges mass, momentum, and energy with the surrounding fluid. To accurately predict the droplet-gas exchange processes, each computational group, which represents a number of droplets with same size,

velocity, position, and temperature, is modelled in Lagrangian coordinates. The position and velocity equations for each computational group written in vector form are

$$\frac{d\vec{x}}{dt} = \vec{v} \quad (9)$$

and

$$\frac{d\vec{v}}{dt} = \frac{3}{8} \frac{\rho}{\rho_l} \frac{|\vec{u} - \vec{v}|}{r_d} (\vec{u} - \vec{v}) C_d \quad (10)$$

where  $\vec{x}$  is droplet position vector and  $C_d$  is the drag coefficient given in terms of Reynolds number of droplet as

$$C_d = \frac{24}{Re_d} (1.0 + 0.166 Re_d^{0.75})$$

and  $\rho_l$ ,  $r_d$ , and  $\vec{v}$  are respectively liquid density, droplet radius, and velocity. Droplet Reynolds number based on droplet diameter and slip velocity between the gas and the liquid is given by

$$Re_d = 2\rho r_d \frac{|\vec{u} - \vec{v}|}{\mu_a(\bar{T})}$$

The temperature in the  $\mu_a$  is replaced by a reference temperature defined as

$$\bar{T} = \frac{T + 2T_d}{3}$$

where  $T$  and  $T_d$  are the gas and droplet temperatures. The rate of change of droplet size is given by

$$\frac{dr_d}{dt} = \frac{-\dot{M}}{4\pi r_d^2 \rho_l} \quad (11)$$

where  $\dot{M}$  is the droplet vaporization rate given by

$$\dot{M} = 4\pi (\rho D)_a r_d [1 + 0.3 Re_d^{1/2} Sc_d^{1/3}] \ln(1+B) \quad (12)$$

$Sc_d$  is the droplet Schmidt number and  $B$  is the mass transfer parameter defined as

$$B = \frac{Y_{fs} - Y_f}{1 - Y_f}$$

The fuel vapor mass fraction at the droplet surface is obtained from

$$Y_{fs}(T_s) = \frac{W_f}{W_f + W_{av} \left( \frac{P}{P_v(T_s)} \right)} \quad (13)$$

$W_{av}$  is the local average molecular weight of all species exclusive of fuel vapor and  $P_v$  is the equilibrium vapor pressure assumed to be equal to the saturated partial pressure at the droplet surface.

Finally, the internal heat transfer mode within the droplet is modelled through the infinite-conduction model as

$$\frac{4}{3} \pi r_d^3 \rho_l C_{pl} \frac{dT_s}{dt} = \dot{M} L(T) + \dot{M} Q_d \quad (14)$$

where

$$Q_d = \frac{K_a (T - T_s)}{(\rho D)_a B}$$

and  $L(T_s)$  is latent heat of vaporization,  $T_s$  the droplet surface temperature, and  $C_{pl}$  the liquid specific heat, and  $(\rho D)_a$  is defined as

$$(\rho D)_a = D_1 \bar{T}^{D_2}$$

where  $D_1$  and  $D_2$  are constants. Subscripts a, d, f, g,  $\ell$ , s, and O designate respectively air, droplet, fuel species, droplet group, liquid phase, droplet surface, and oxygen species.

### Boundary and Initial Conditions:

Referring to Fig. 1, the boundary and initial conditions are given as follows:

Gas-Phase: at  $t=0$ ,

$$Y_f = 0, Y_{O_2} = 0.23, Y_{N_2} = 0.77, \text{ and } T = 400K$$

For  $0 \leq r \leq L, Z=0$

$$Y_f = 0.0, Y_{O_2} = 0.0, Y_{N_2} = 1.0, \text{ and } T = 400K$$

For  $L \leq r \leq R, Z=0$

$$Y_f = 0.0, Y_{O_2} = 0.23, Y_{N_2} = 0.77, \text{ and } T = 400K$$

For  $0 < r < R, Z=0.0$

$$u = 30 \text{ cm/s}, v = 0$$

For  $0 < r < R, Z=H$

$$P = P_{atm}$$

For  $0 < Z < H, r=0$

$$\frac{\partial u}{\partial r} = \frac{\partial v}{\partial r} = \frac{\partial I}{\partial r} = \frac{\partial Y_i}{\partial r} = 0.0$$

For  $0 \leq Z \leq H, r=R$

$$u = v = 0.0, T = 400K, \text{ and } \frac{\partial Y_i}{\partial r} = 0$$

Here  $u$  and  $v$  are the axial and radial gas velocity components respectively.

Liquid-Phase:

$$T_s = 300K, r_{di} = 15 \mu m, u_d = 35 \text{ cm/s}, v_d = 0.0, \text{ and } x_d = z_d = 0$$

where  $u_d$ ,  $v_d$ ,  $z_d$ , and  $x_d$  are the axial and radial droplet velocities and positions at injection. In addition to specifying the droplet velocity, size, and temperature at injection, the liquid mass of each droplet group and the number of droplets per group need to be specified as well. For two-dimensional axisymmetric computations, about 2000 droplet groups are generally adequate to represent the continuous droplet size distribution and yield satisfactory results. In the present computations, 3000 droplet groups are specified at injection. By dividing the liquid mass flow, to be injected for stoichiometric conditions, by the number of droplet groups, the mass of each droplet group is obtained. The number of droplets per group  $n$  is then determined from the relation

$$M_g = \frac{4}{3} \pi r_d^3 \rho_l n$$

where droplets are assumed to be spherical. Note that for monodisperse spray injection  $r_d$  is specified, whereas for polydisperse spray injection  $r_d$  is selected from a droplet size distribution by random sampling using Monte Carlo method.

### III. NUMERICAL PROCEDURE

The conservation equations of mass species, continuity, momentum, and energy for the gas-phase and droplet position, velocity, size, and temperature for the liquid-phase are solved numerically via the KIVA-II computational algorithm of Amsden et al.<sup>21</sup>. The equations are integrated using the control volume approach. The computational grid is made up of arbitrary shaped hexahedrons cells whose vertices coordinates are referenced with respect to a fixed system of Cartesian coordinates and can either be specified to be fixed in space (Eulerian) or moving (Lagrangian). The volume of a hexahedron is computed by dividing it into five tetrahedrals and calculating the volume of each tetrahedral and then summing. A cell surface area is computed by dividing the surface into four nonplanar triangles and calculating each triangle surface area and then adding them up. A block

of ten cells, two and five in the radial and axial directions respectively, are assigned to be the ignition source. Ignition energy is deposited in these cells for a certain duration of time. The amount of ignition energy, duration, and location of the ignition source are determined by numerical experiments such that a flame kernel can be created and leads to a self-sustained combusting situation. Note that the ignition parameters are very critical for determining the state of the established flame kernel and the resulting combustion wave. For instance, turning off the ignition source before burning becomes self-supported can result in a flame lift-off situation due to thermal losses by diffusion from the flame kernel.

In an earlier investigation<sup>10</sup>, we reported some results computed by using the original KIVA-II code for the gaseous diffusion flame case. It was shown that the original algorithm failed to predict the steady-state solution. In brief, the problem was that pressure waves were being continuously sent into the computational domain by the outflow boundary. The effect of these pressure waves was even felt in the upstream flow and as a result it precluded the attainment of a steady-state solution. This problem was corrected by accounting for the pressure forces acting on the outflow boundary from the atmospheric pressure side for the boundary velocities. More details regarding these modifications can be found in Ref. 10. A number of residual criteria were employed to check the predictions of the modified version for the attainment of the steady state solution and all showed good results within the convergence tolerances specified. In the present study, the modified version of the KIVA-II code is used and the results were checked for steady-state solutions. Figure 2 shows the total residual in the velocity field plotted against time for the momodisperse, single step reaction scheme (Results and Discussions Section). The steady-state solution is clearly seen to be reached.

Finally, since KIVA-II solves the finite difference approximations of a given problem in its physical space (i.e., no coordinate transformation), the two-dimensional axisymmetric

computations are carried out in a cylindrical sector referenced with respect to the Cartesian coordinates  $x$ ,  $y$ , and  $z$ . The computational grid employed here consisted of  $50 \times 1 \times 90$  cells which yielded results that are grid-size independent. The time step size used varied from  $10^{-5}$  to  $10^{-6}$  s. The CPU time needed to obtain a steady-state solution was about 14 hours on the Cray-YMP at NASA Lewis Research Center.

#### IV. RESULTS AND DISCUSSIONS

As stated earlier that the primary objective of the present study is to carry out a detailed numerical simulation of laminar spray diffusion flames by accounting for most of physical and chemical processes of the gas-phase and their interaction with the liquid-phase. However, in order to appreciate the effect of introducing the fuel in the form of liquid sprays on the the structure of the flame, some of the numerical computations for purely gaseous fuels, we reported previously<sup>10</sup>, will be presented here for the purpose of comparison. The comparison will, however, be limited for a situation where the numerical simulations are made both for gaseous and spray flames under the same stoichiometry, initial and boundary conditions. In addition, some calculations for the case of introducing the fuel in *both* liquid and gaseous forms will also be presented here.

The fuel selected for this study is octane. The chemical parameters used here and the equilibrium reactions are all given in Appendix A. Computations are made only for stoichiometric conditions. Results for a monodisperse droplet stream with only one-step reaction (i.e., no equilibrium reactions) will be given first.

##### 1. Monodisperse/Single Step-Reaction

The injected spray in this case is assumed to have undergone initial break-up and thus only droplets of  $30 \mu\text{m}$  in diameter are continuously injected. Collision between droplets is not considered and the droplets are assumed to have initially only an axial

velocity component. The global structural features of the steady-state spray diffusion flame represented by the temperature and concentration fields are shown in Figs. 3a-3c. The corresponding fields for the gaseous diffusion flame are shown in Figs. 4a-4c. The Z-axis is the center line of the two concentric tubes and X-axis is the radial coordinate. First, regarding the steady-state spray flame, it is seen that regions of high temperatures have developed and appear to occupy a significant portion of the flow field. Temperatures ranging from 400 K at the wall to 2104 K are present and indicate the presence of large temperature gradients. The results also show that the fuel and oxygen species do not seem to coexist in the high temperature regions; only in a small region near the inflow boundary. Large temperatures occur at the interface of the fuel and oxygen sides. The maximum temperature is seen to occur at the location of stoichiometry on the fuel side and hot products diffuse radially outward on both sides of that location. The sharp variations in the temperature field are clearly indicative of a burning distribution, being zero at the wall and maximum at the center of the 2100 K contour. Furthermore, the temperature contours illustrate the finite thickness of the flame zone. Thus, spray flames do possess a finite thickness and never collapse onto a surface as implied by the flame-sheet model. The maximum fuel vapor concentration is 0.56 and is located at about  $Z=1.1$  cm. This indicates that complete vaporization of the liquid droplets occurs at that location. In fact, no droplets exist beyond that location.

Secondly, in regard to the comparison between the spray and gaseous flames, the temperature field both for the gaseous as well as for the spray flames are shown in Figs. 3a and 4a respectively. It can be seen that the spray flame has large regions of high temperatures compared to the gaseous flame. The 1900 K contour, Fig. 3a, for instance, is seen to be significantly longer than the corresponding one for the gaseous flame and is displaced more towards the center line. The 2100 K contour for the spray flame appears to occur well above the inflow boundary. These observations indicate that the spray flame



would be longer and narrower than that of the gaseous one. Note that this has also been predicted in Ref. 19, however, for 80% liquid and 20% vapor. Moreover, as indicated by the spray flame temperature contours, the flame is relatively narrow near the inlet and becomes broader near the outlet of the combustor. This is clearly indicative of the flame stabilization mechanism which considerably differs from that of the gaseous flame. In the gaseous flame, for example, the flame is established and then stabilized at or adjacent to the interface of the combustible gas-air streams near the inlet. The spray flame, however, is observed to be stabilized in the laminar flow well above the inflow boundary.

The fuel concentration fields of the spray and gaseous flames are shown in Figs. 3b and 4b respectively. It is seen that while the maximum concentration of fuel vapor for the gaseous flame is in the immediate proximity of the inflow boundary, the maximum concentration for the spray flame occurs farther downstream above the combustor inlet. This is a result of the fact that the liquid droplets must travel some distance in the field before they are completely vaporized. The immediate effect of replacing a gaseous fuel by a liquid one is therefore a change in the location of the maximum fuel vapor source and consequently lifting of the flame. Since most of the fuel vapor in the spray flame is located downstream of the inflow boundary, radial diffusion of fuel towards the wall near the inflow boundary is restricted due to the presence of a flame. As a result, more fuel vapor is convected upward for the spray flame compared to that of the gaseous flame which in turn leads to a longer flame. It is also important to observe that some oxygen in the spray flame appears to flow out of the combustor, Fig. 3c. In contrast, the gaseous flame shows no oxygen leaving the combustor, Fig. 4c. This reinforces our earlier observation that the spray flame is taller and narrower than the gaseous flame.

Figures 5a-5b show the radial profiles of the axial velocity at various locations downstream for the gaseous and spray flames respectively. It is clearly seen that the velocity profile of the gaseous flame has developed to a parabolic one at  $z=5$  cm. However, the

velocity profile of the spray has not yet become parabolic at the same location, which develops to parabolic at  $z=8.7$  cm, and resembles that of the gaseous at  $z=3$  cm. This is primarily caused by the flame stabilization mode for the spray case. The distinct difference in the velocity profiles of the gaseous and spray flames can be related to the flame shape development, i. e. , as the flame front moves towards the center line, the reactants species flow to the flame front where they react and products are generated.

To further understand the difference in the radial velocity profiles, the gaseous and spray flame shapes are shown in Fig. 6a-6b respectively. Note that the flame shape is obtained by calculating the loci of the maximum temperature (see Ref. 10). The spray flame is substantially different from that of the gaseous one. While the gaseous flame maintains its width from the inlet to almost  $2/3$  of its height and then converges towards the center line, the spray flame is seen to diverge (opens up) initially, followed by a constant width and finally begins to converge towards the center line. The spray flame is also quite longer than the gaseous flame as anticipated earlier. Thus, the immediate impact of introducing the fuel as liquid is considerable changes in the flame dimensions. Figure 6b also exhibits the droplets trajectories in the flow field. The droplets, which are injected vertically upward, appear to cluster and be deflected to form a hollow cone shape-like injector and then follow almost straight trajectories as they become suspended in the laminar flow. It is observed that after the droplets travel some distance downstream, they experience a significant loss of mass due to vaporization and when droplet's mass becomes less than 1% of its initial mass it is discarded.

## **2. Monodisperse with Equilibrium Reactions**

The combustion characteristics and flame behavior are a result of a large number of coupled physical and chemical elementary processes. The use of a one-step global reaction scheme to model chemistry in combustion is merely a gross approximation to the real

multistep reactions occurring in combustion systems. The elementary reactions for most hydrocarbon fuels are unfortunately not yet known. There are, however, two types of reactions, namely kinetic and equilibrium reactions. For high temperature situations, the kinetic and equilibrium reactions are present and proceed simultaneously, but at different rates. The computations presented earlier for a one-step reaction illustrated the existence of high temperatures spanning a significant portion of the flow field. It is therefore believed that the use of equilibrium reactions along with a one-step reaction is of great interest, since their use implies changes in the concentration field and consequently flame characteristics. For brevity, results for the one-step reaction without and with equilibrium reactions will be referred to respectively as scheme 1 and 2 hereafter.

Figures 7a-7c show the steady-state temperature, fuel vapor, and oxygen mass fraction contours for scheme 2. It is seen that while the global qualitative features of the flame structure are similar to those of scheme 1, significant quantitative differences are predicted. In particular, the temperature contours show a decrease in temperature as compared to that of scheme 1 (i.e., the absence of the 2100 K contour). Note that the maximum temperature for scheme 2 is 2001 K. Further, the flame zone appears to have moved downward. This is mainly reflected in the 1900 and 1700 K contours. The implication is that the flame would be shorter than that for scheme 1. The downward movement of the flame zone is primarily due to the increase in its surface area. This phenomenon is known as a flame broadening and is caused by "equilibrium broadening influence"<sup>23</sup>. Corresponding changes in the oxygen and fuel vapor contours are also seen in Figs 7b and 7c. The maximum fuel vapor concentration, for example, is now at  $Z = 0.8$  cm for scheme 2, whereas for scheme 1 it is at  $z = 1.22$  cm. Therefore, the immediate effect of introducing equilibrium reactions is a reduction in the temperature field with a corresponding movement of the flame zone. Note that the decrease in the temperature results in enhancing the radial diffusion of reactants into the flame zone (or decreasing the axial diffusion) and thus

stretching the flame zone.

To further demonstrate the influence of allowing for equilibrium reactions along with a one-step reaction, radial profiles of the axial velocity at four stations downstream are plotted in Fig. 8. It is clearly seen that at  $z=5$  cm, the velocity profile is close to parabolic as compared to that of scheme 1 which becomes parabolic at  $z=8.7$  cm. This is a direct consequence of the equilibrium broadening effect, since convective flow is a strong function of temperature and an increase in the rate of diffusion of the reactants into the flame zone implies a decrease in the convective flow<sup>24</sup>.

The fact, that the flow field has developed to parabolic, implies that the flame front converges to the center line of the two concentric tubes. This is illustrated in Fig. 9. An interesting feature of the predicted flame here is its tip shape, which is substantially different from that of the gaseous flame shape. In fact, the predicted flame shape here is in good agreement with the experimentally observed flame<sup>15</sup> for an iso-octane full cone spray. This substantiates our earlier observation regarding the significant impact of introducing the fuel in the form of liquid sprays on the flame shape and dimensions as compared to that of the pure gaseous case.

### 3. Polydisperse with Equilibrium Reactions

Since in practical situations polydisperse sprays are used, it is of interest to study the effect of the spray character on the flame behavior. However, results for the flame shape will only be presented here. Figure 10 shows the flame shape and drops trajectories for a polydisperse spray injection for scheme 2. In predicting this flame, the computations are carried out starting from the monodisperse case after replacing the injection model. The liquid mass flow rate for the polydisperse spray is kept the same as that for the monodisperse case to preserve the overall unity equivalence ratio. Note that the  $\chi$ -squared distribution for droplet size is used here and the SMD is  $30 \mu\text{m}$ . The flame shape and

dimension are surprisingly seen to be unaffected by the injection of a polydisperse spray. This is believed to be due to maintaining the SMD at  $30\ \mu\text{m}$ , which is the diameter for the monodisperse case. However, the drops trajectories are modified and appear to form again a hollow cone-like injection mode. Droplets of sizes between  $40\text{-}60\ \mu\text{m}$  travel further downstream, since they possess more momentum than those of smaller sizes.

#### 4. Monodisperse Gaseous-Spray/One-Step Reaction

Some calculations for a mixture of 80% liquid in the form of monodisperse droplets and 20% in the gaseous form by mass are performed. The choice of an 80-20% liquid-gaseous mixture is somewhat arbitrary as far as the numerical simulations are concerned. However, the analytic solution of Ref. 20 predicts flames almost twice as tall as those for the pure gaseous case. It is therefore of interest to investigate the flame characteristics and dimensions for this particular mixture and compare the results with those of pure liquid and gaseous flames under the same conditions.

Figures 11a-11c illustrate the temperature, fuel vapor, and oxygen mass fractions contours for the steady-state solution. It is seen that important structural changes have emerged from the introduction of 20% gaseous fuel. The 2100 K contour is now absent. Similar changes in the 1900 and 1700 K contours are apparent. The net effect is to displace the flame zone outward radially to lie more towards the oxidizer side and more importantly is its close resemblance to the pure gaseous flame structure. Moreover, the radial movement of the flame zone appears to be somewhat uniform along the combustor and indicates the cylindrical shape of the flame. This is further reflected in the fuel vapor mass fraction contours. The contours exhibit an almost cylindrical distribution of the fuel vapor from the inlet to the outlet of the combustor. The flame is located at the interface of the fuel and oxidizer regions. The fuel and oxygen fields again show no significant overlap between the two species.

The outward radial movement of the flame zone is believed to be caused by the radial diffusion of the fuel species. The ability of the fuel vapor to diffuse outwardly in such a manner is due to the presence of essentially two sources of fuel vapor. In the immediate vicinity of the inflow boundary, gaseous fuel is present, which is responsible for the initial radial diffusion. Further downstream, the spray droplets vaporize producing fuel vapor along their trajectories as they travel. Note, however, that due to the high temperature presence in the vicinity of the the inflow boundary, the spray droplets vaporize faster than that of the pure spray case.

To illustrate the effect of introducing the fuel in both liquid and gaseous forms on the flame shape and dimensions, the flame shapes for pure gaseous, spray, and gaseous-spray fuels are plotted in Fig. 12. It is clearly observed that near the inflow boundary, the gaseous-spray flame shape lies between the pure gaseous and spray flames, as expected. However, the flame at this location resembles more that of the gaseous one, indicating the dominant effect of introducing a gaseous fuel along with a spray. In fact, the flame front follows closely that of the gaseous one up to the middle of the combustor. Further downstream the spray effects become dominant. It is also interesting to note that the length of the gaseous-spray flame lies between that of pure spray and gaseous flames. Another important observation is that the gaseous-spray mixture considered here does not appear to produce flames twice as long as those of pure gaseous ones as was indicated in Ref. 20. The flame is *only* 16% longer than that of the gaseous flame. Furthermore, significantly longer gaseous-spray flames can only be accomplished by increasing the inflow velocity of gaseous vapor and the spray droplets. However, stabilizing the flame becomes a critical issue unless other means, i.e., a flame holder, are introduced. In addition, one must precisely determine the flow Reynolds number for which the flow remains laminar so that the physics of the laminar flames are not violated.

## V. CONCLUSION

Laminar spray diffusion flames are studied numerically by solving the gas-phase conservation equations for species, mass continuity, momentum, and energy and the liquid-phase equations for droplet position, velocity, size, and temperature. The interactions between the two phases are represented as source/sink terms in the gas-phase governing equations. The spray is represented by both monodisperse as well as polydisperse droplets. The numerical modelling is performed using an existing computer code, KIVA-II.

The numerical results clearly show the distinct effect of introducing the fuel in the form of sprays on the flame structure. In particular, spray flames are predicted to be taller and narrower than the gaseous ones, primarily due to the evaporation of the spray droplets. Moreover, spray flames are found to have a cylindrical shape, in agreement with experimentally observed shapes. Flame shape and dimensions are surprisingly found to be unaffected by the method the spray is modelled, i.e., monodisperse or polydisperse sprays, and thus more analyses are needed to clarify this aspect.

The numerical computations further demonstrate a marked influence with the use of equilibrium reactions along with a one-step global reaction scheme. The introduction of equilibrium reactions is found to decrease the flame temperature and consequently increasing the surface area of the flame zone and reducing its length. The increase in the flame zone surface area is due to a phenomenon termed "equilibrium broadening". The results also show that spray flames do possess a finite thickness. However, the overlap between the reactant species is found to be much smaller than that of the purely gaseous flames.

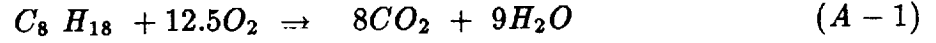
The simulations for the case of introducing a mixture of gaseous-spray exhibit that the flame shape is rendered less cylindrical as compared to that produced by a pure spray. Moreover, wider flame zone is predicted due to the presence of two sources of fuel vapor at two distinct locations in the combustor. Finally, the results show no flames twice as tall

as that of pure gaseous flames for an 20-80% gaseous-liquid mixture as indicated in Ref. 20. In fact, the flame length is found to lie between that of pure gaseous and liquid. Thus, further analyses should be performed to enlighten this nebulous aspect. As a final note, it should be stated that the numerical simulations presented here clearly indicate that under certain conditions, it is possible to produce stable Burke-Shumann type laminar flames with liquid fuel sprays. This should motivate further experimental work in producing stable laminar spray flames for more fundamental studies of such flames.



## APPENDIX A

The octane fuel reaction is governed by a global one-step reaction of the form



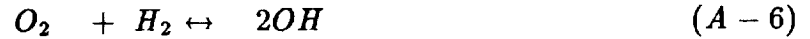
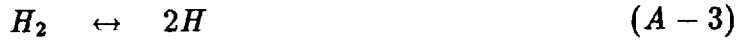
The reaction rate expression is given by

$$\dot{\omega} = k_{fr} \prod_i \left( \frac{\rho_i}{W_i} \right)^{a_i} \quad (A - 2)$$

The reaction rate constant  $k_{fr}$  is determined from the Arrhenius expression as

$$k_{fr} = A \exp(-E/R_u T)$$

$E$  is the activation energy taken as 25.6 kcal/mole and  $A$  is the preexponential factor taken  $10^{12}$ . Six equilibrium reaction are considered here and these are



The equilibrium reactions constant is given by

$$\prod_i \left( \frac{\rho_i}{W_i} \right)^{\nu_{i,r} - \nu_{i,r}} = k_c(T)$$

where  $k_c(T)$  is the equilibrium constant and  $\nu_{il,ir}$  are the stoichiometric coefficients of  $i$ th species on the left and right sides of each reaction. The chemical source term in the species equation is given by

$$\rho_c = W_i \sum_r (\nu_{ir} - \nu_{il}) \dot{\omega} \quad (A - 9)$$

and the chemical source term in the energy equation is given by

$$Q_c = \sum_r \sum_i (\nu_{ir} - \nu_{il}) (\Delta h_f^o)_i \dot{\omega} \quad (A - 10)$$

$(\Delta h_f^o)_i$  is the heat of formation of the  $i$ th species and the values are taken from JANAF tables. The source/sink terms due to spray gas interaction are given by

$$\rho_s = \frac{1}{V} \sum_1 N_g \dot{M} \quad (A - 11)$$

where  $V$  is the cell volume in which a droplet group is located and  $N_g$  is the number of droplet groups. The momentum equation for the liquid-phase is given by

$$\vec{F}_s = \frac{1}{V} \sum_1 N_g (4/3 \pi \rho_l r_d^3 \frac{d\vec{v}}{dt} + \dot{M} \vec{v}) \quad (A - 12)$$

where the first term represents droplet's acceleration and the second term is the momentum associated with droplet vaporization.

Finally, the spray source term in the energy equation is given as

$$Q_s = \frac{1}{V} \sum_i N_g [\dot{M} I_\ell(T_d) + \dot{M}/2(\vec{v} - \vec{u})^2 + 4/3 \pi r_d^3 \rho_l C_{pl} \frac{dT_s}{dt} + 4/3 \pi r_d^3 \frac{d\vec{v}}{dt} \cdot (\vec{v} - \vec{u})] \quad (A - 13)$$

where  $I_\ell$  is the liquid internal energy at  $T_d$  temperature and  $C_{pl}$  is the liquid specific heat and both are taken from JANAF table.

## REFERENCES

1. Burke, S.P.; and Shumann, T.E.W.: Diffusion Flames. *Ind. Eng. Chem.*, vol. 20, no. 10, 1928, pp. 998-1057.
2. Clarke, J.F.: Hydrogen Diffusion Flames. *J. Inst. Math. Its Appl.*, vol. 3, 1967, pp. 283-302.
3. Clarke, J.F.: Equilibrium Chemistry-Diffusion Flames. *Proc. R. Soc. London, A*, vol. 307, 1968, pp. 283-302.
4. Chang, S.H., and Law, C.K.: Streamwise Effects on Diffusion Flames. *Combust. Sci. Technol.*, vol. 37, 1984, pp. 21-46.
5. Penner, S.S.; Bahadori, M.Y.; and Kennedy, E.M.: Effects of Variable Diffusion Coefficients on Burke-Schumann Flames. *Dynamics of Flames and Reactive Systems, Progress in Astronautics and Aeronautics*, Vol. 95, J.R. Bowen, ed., AIAA, New York, 1984, pp. 262-269.
6. Bahadori, M.Y.; Li, C.-P.; and Penner, S.S.: Two Adjacent Coupled Laminar Diffusion Flames With Cylindrical Symmetry. *Dynamics of Reactive Systems, Pt. 1: Flames and Configurations, Progress in Astronautics and Aeronautics*, Vol. 105, J.R. Bowen, J.-C. Leyer, and R.I. Soloukhin, eds., AIAA, New York, 1986, pp. 192-207.
7. Li, C.-P.; Wiesenmann, D.; and Penner, S.S.: Coupled Laminar Diffusion Flame With Variable Properties. *Combust. Flame*, vol. 65, 1986, pp. 215-225.
8. Gosman, A.D.; et al.: *Heat and Mass Transfer in Recirculating Flows*. Academic Press, New York, 1969.
9. Mitchell, R.E.; Sarofim, A.F.; and Clomburg, L.A.: Experimental and Numerical Investigation of Confined Laminar Diffusion Flames. *Combust. Flame*, vol. 37, 1980, pp. 227-244.
10. Mawid, M.A.; Bulzan, D.L.; and Aggarwal, S.K.: A Detailed Numerical Investigation of Burke-Schumann Gaseous and Spray Flames. AIAA Paper 91-2311, 1991.

11. Ellzey, J.L.; Laskey, K.J.; and Oran, E.S.: A Study of Confined Diffusion Flames. *Combust. Flame*, vol. 84, 1991, pp. 249-264.
12. Chigier, N.: Atomization and Spray Research for Gas Turbine Engines. Israel Annual Conference on Aviation and Astronautics, 30th, Israel Institute of Technology, Haifa, Israel, 1989, pp. 120-124.
13. Greenberg, J.B.; Albagli, D.; and Tambour, Y.: An Opposed Jet Quasimonodisperse Spray Diffusion Flame. *Combust. Sci. Technol.*; vol. 50, no. 4-6, 1986, pp. 255-270.
14. Greenberg, J.B.; and Tambour, Y.: Far-Field Coalescence Effects in Polydisperse Spray Jet Diffusion Flames. Twenty-First Symposium (International) on Combustion, The Combustion Institute, Pittsburgh, PA, 1986, pp. 655-663.
15. Moore, J.G.; and Moore, J.: The Distributions of Temperature and Major Species in Laminar Diffusion Flames. The Sixteenth Symposium (International) on Combustion, The Combustion Institute, Pittsburgh, PA, 1977, pp. 1123-1132.
16. Harsha, R.T.; and Edelman, R.B.: Analytic Modeling of a Spray Diffusion Flame. AIAA Paper 84-1317, 1984.
17. Mao, C.P.; Szekely, G.A.; and Faeth, G.M.: Evaluation of a Locally Homogeneous Flow Model of Spray Combustion. *J. Energy*, vol. 4, Mar.-Apr. 1980, pp. 78-87.
18. Kim, J.B.; and Sichel, M.: Diffusive Burning of a Plane Liquid or Spray Jet. Presented at the Fall Technical Meeting, Eastern Section of the Combustion Institute, Gaithersburg, MD, 1987.
19. Greenberg, J.B.: The Burke-Schumann Diffusion Flame Revisited - With Fuel Spray Injection. *Combust. Flame*, vol. 77, Sept. 1989, pp. 229-240.
20. Greenberg, J.B.: Spray Diffusion Flames With Arbitrary Initial Droplet Velocity Distributions. *Combust. Sci. Technol.*, vol. 75, 1991, pp. 13-30.

21. Levy, Y.; and Bulzan, D.L.: Laminar Spray Combustion Presented as a Poster at the International Conference on Liquid Atomization and Spray System, Washington, DC, July 15th, 1991.
22. Amsden, A.A.; O'Rourke, P.J.; and Butler, T.D.: KIVA-II: A Computer Program for Chemically Reactive Flows With Sprays. Report LA-11560-MS, Los Alamos National Laboratory, NM, 1989.
23. Stull, D.R.; Prophet, H.; and Chase, M.W.: JANAF Thermochemical Tables. Third ed. American Chemical Society, Washington, DC, 1986.
24. Peters, N.; and Williams, F.A.: Effects of Chemical Equilibrium on the Structure and Extinction of Laminar Diffusion Flames. Dynamics of Flames and Reactive Systems, Progress in Astronautics and Aeronautics, Vol. 95, J.R. Bowen, ed., AIAA, New York, 1984, pp. 37-60.
25. Warnatz, W.T.; and Peters, N.: Stretch Effects in Planar Premixed Hydrogen-Air Flames. Dynamics of Flames and Reactive Systems, Progress in Astronautics and Aeronautics, vol. 95, J.R. Bowen, ed., AIAA, New York, 1984, pp. 61-74.

# REPORT DOCUMENTATION PAGE

Form Approved  
OMB No. 0704-0188

Public reporting burden for this collection of information is estimated to average 1 hour per response, including the time for reviewing instructions, searching existing data sources, gathering and maintaining the data needed, and completing and reviewing the collection of information. Send comments regarding this burden estimate or any other aspect of this collection of information, including suggestions for reducing this burden, to Washington Headquarters Services, Directorate for Information Operations and Reports, 1215 Jefferson Davis Highway, Suite 1204, Arlington, VA 22202-4302, and to the Office of Management and Budget, Paperwork Reduction Project (0704-0188), Washington, DC 20503.

<b>1. AGENCY USE ONLY (Leave blank)</b>		<b>2. REPORT DATE</b> February 1993	<b>3. REPORT TYPE AND DATES COVERED</b> Technical Memorandum	
<b>4. TITLE AND SUBTITLE</b> Structure of Confined Laminar Spray Diffusion Flames/Numerical Investigation			<b>5. FUNDING NUMBERS</b>  WU-505-62-21	
<b>6. AUTHOR(S)</b> M.A. Mawid, D.L. Bulzan, and S.K. Aggarwal				
<b>7. PERFORMING ORGANIZATION NAME(S) AND ADDRESS(ES)</b>  National Aeronautics and Space Administration Lewis Research Center Cleveland, Ohio 44135-3191			<b>8. PERFORMING ORGANIZATION REPORT NUMBER</b>  E-7193	
<b>9. SPONSORING/MONITORING AGENCY NAMES(S) AND ADDRESS(ES)</b>  National Aeronautics and Space Administration Washington, D.C. 20546-0001			<b>10. SPONSORING/MONITORING AGENCY REPORT NUMBER</b>  NASA TM-106038 ICOMP-93-2	
<b>11. SUPPLEMENTARY NOTES</b> M.A. Mawid, Institute for Computational Mechanics in Propulsion, NASA Lewis Research Center (work funded under NASA Cooperative Agreement NCC3-233). ICOMP Program Director, Louis A. Povinelli, (216) 433-5818; D.L. Bulzan, NASA Lewis Research Center and S.K. Aggarwal, The University of Illinois at Chicago, Chicago, Illinois 60680 and Institute for Computational Mechanics in Propulsion, NASA Lewis Research Center, Cleveland, Ohio (work funded under NASA Cooperative Agreement NCC3-233). Responsible person, M.A. Mawid, (216) 433-5965.				
<b>12a. DISTRIBUTION/AVAILABILITY STATEMENT</b>  Unclassified - Unlimited Subject Category 34			<b>12b. DISTRIBUTION CODE</b>	
<b>13. ABSTRACT (Maximum 200 words)</b> <p>The structure of confined laminar spray diffusion flames is investigated numerically by solving the gas-phase conservation equations for mass species, continuity, momentum, and energy and the liquid-phase equations for droplet position, velocity, size, and temperature. A one-step global reaction scheme along with six equilibrium reactions are employed to model the flame chemistry. Monodisperse as well as polydisperse sprays are considered. The numerical results demonstrate that liquid spray flames substantially differ from gaseous flames in their structure, i.e., temperature, concentration, and velocity fields, shape, and dimensions under the same conditions. Spray flames are predicted to be taller and narrower than their counterpart gaseous ones and their shapes are almost cylindrical, in agreement with experimental observations. The numerical computations also show that the use of the equilibrium reactions with the one-step reaction scheme decreases the flame temperature compared to the one-step reaction scheme without the equilibrium reactions and more importantly increases the surface area of the flame zone due to a phenomenon termed "equilibrium broadening". The spray flames also possess a finite thickness with minimal overlap of the fuel and oxygen species. A case, for which a fuel-mixture consisting of 20 to 80 percent gas-liquid by mass is introduced into the combustor, is also investigated and compared with predictions using only gaseous or liquid fuel.</p>				
<b>14. SUBJECT TERMS</b> Laminar spray flames; A numerical investigation; 2D computations; Monodisperse sprays			<b>15. NUMBER OF PAGES</b> 28	
			<b>16. PRICE CODE</b> A03	
<b>17. SECURITY CLASSIFICATION OF REPORT</b> Unclassified	<b>18. SECURITY CLASSIFICATION OF THIS PAGE</b> Unclassified	<b>19. SECURITY CLASSIFICATION OF ABSTRACT</b> Unclassified	<b>20. LIMITATION OF ABSTRACT</b>	